Title: An axon initial segment sodium channel $Na_v1.2$ regulates sleep homeostasis

Authors: Yu Li[1*], Juhang Liu[1*], Kaiyue Yan[1*], Huiwen Tian[1], Chongchong Zhao[1], Qiang Sun[1], Guangfu Wang[1†], Jing Ma[1†] and Zhiqiang Wang[1†]

Affiliations:

[1]The HIT Center for Life Sciences, School of Life Science and Technology, Harbin Institute of Technology, Harbin, 150001, China

[*]These authors contributed equally to this work.

[†]Correspondence:
Zhiqiang Wang: zhiqiang.wangmj@foxmail.com,
Jing Ma: jingmawzq@foxmail.com,
Guangfu Wang: wangguangfu@hit.edu.cn

Abstract: The slow-wave activity of non-rapid-eye-movement sleep reflects system-wide oscillation of cortical neurons and sleep need, which underlies a tight genetic control. Here, we identify a mutation in sodium channel $Na_v1.2$ that affects channel's slow inactivation and daily sleep need in mice. Moreover, this mutation leads to markedly reduced phosphorylation changes of brain proteome and rebound of slow-wave activity after sleep deprivation, highlighting a role of $Na_v1.2$ in sleep homeostasis regulation.

MAIN TEXT

An understanding of the regulatory mechanism of sleep is crucial for elucidating the relationship between sleep and cognitive function, along with overall physiological health. Genetic studies have identified several sleep-controlling protein kinases and phosphatases, such as SIK3[1,2], ERK1/2[3], CaMKII[4,5], PKA[6,7], PP1 and calcineurin[7] in the regulation of duration, timing, architecture and homeostasis of sleep in mammals. Thus, to elucidate the downstream effectors for these signalling pathways needs to be carried out. Multiple quantitative phosphoproteomic analyses have revealed a large-scale phosphoprotein, the phosphorylation status of which is closely linked to sleep–wake states[8-12]. Particularly, we identified 80 Sleep-Need-Index-PhosphoProteins (SNIPPs) by cross-comparison of two increased sleep need models, *Sleepy* and sleep-deprived models[12]. The genetic changes of 12 SNIPPs cause sleep phenotypes in mice or humans, suggesting that the SNIPPs likely contain unknown sleep regulators[12].

While 69 SNIPPs could be annotated as synaptic proteins suggesting a mechanistic link between the synaptic homeostasis and sleep–wake homeostasis[12,13], we also noticed that *Scn1a* and *Scn2a*, which encode sodium channel $Na_v1.1$ and $Na_v1.2$ as axon initial segment (AIS) proteins in the non-synaptic category (Fig. 1a), and were predominantly expressed in inhibitory neurons or excitatory neurons[14,15], respectively. Further analysis also revealed that the phosphorylation status of 132 AIS proteins is dynamically regulated in either *Sleepy* or sleep-deprived models (Extended Data Fig. 1a-d, Supplementary Table 1). However, the role of these AIS proteins in mammalian sleep regulation is not yet fully understood.

Slow-wave activity (SWA), which refers to the delta power (Hz 1–4) of electroencephalogram (EEG) during non-rapid-eye-movement sleep (NREMS), represents one the best markers for the sleep–wake homeostasis[12,16]. We have already identified 13 SWA-SNIPPs that are common in three models with increased SWA (MK801, *Sleepy* and sleep-deprived) and accumulate their phosphorylation in a time-dependent manner[12] (Extended Data Fig. 1e). 11 SWA-SNIPPs, such as Bassoon, Synapsin-1 and RIMS1, are synaptic proteins that regulate neurotransmitter release

and short-term synaptic plasticity (Extended Data Fig. 1e). Additionally, $Na_v1.2$, which is crucial for action potential propagation in excitatory neurons[14], may contribute critically to the regulation of SWA or sleep need by controlling cortical network synchronization and global slow oscillations[16,17]. We found that most significantly increased phosphorylation sites of $Na_v1.2$ are clustered in a functional patch and located in an intracellular loop between transmembrane domains (DI–II) (Fig. 1b, Supplementary Table 2). Previous cellular level studies reported that the phosphorylation-patch is critical for the regulation of channel's slow inactivation[18,19]. Increased phosphorylation promotes the transition of $Na_v1.2$ into a slow inactivation state, while amino acid asparagine (N1467) in the S6 segment of domain III gates this process, and when mutated to aspartic acid (N1467D) inhibits this state transition[19] (Fig. 1b).

To elucidate the function of $Na_v1.2$ in sleep regulation, we created *Scn2a*^{N1467D} mutant mice (Extended Data Fig. 1f). However, the homozygous mutants exhibited neonatal lethality within 48 hours after birth (Extended Data Fig. 1g), which was consistent with the situation of *Scn2a-null* mice[20]. In contrast, the heterozygous *Scn2a*$^{N1467D/+}$ mice (*N1467D/+*) were healthy, fertile and with a normal body weight (Extended Data Fig. 1h). The *N1467D/+* mice exhibited a significant reduction in the NREMS delta power at baseline level, and showed a certain trend after sleep deprivation despite having a normal sleep amount (Extended Data Fig. 1i-w). To establish a *Scn2a*^{N1467D} homozygous model, we developed an additional strain *Scn2a*$^{fl/fl}$ by inserting loxp sites downstream of exon 3 and upstream of exon 6 (Fig. 1c and Extended Data Fig. 2a, b). By crossing *Scn2a*$^{N1467D/+}$ and *Scn2a*$^{fl/fl}$ mice with CAGG$^{Cre\text{-}ERTM}$ transgenic mice, we obtained a *Scn2a*$^{N1467D/fl}$; CAGG$^{Cre\text{-}ERTM/+}$ mouse strain (*N1467D*) (Fig. 1c). After tamoxifen induction at 6 weeks, we found the $Na_v1.2$ protein amounts were reduced to ~50% compared with wild-type mice (WT) brain samples (Fig. 1c, d), which indicates that only the $Na_v1.2$ N1467D proteoform exists in *N1467D* subjects.

Pyramidal neurons within layer 5 of the neocortex regulate SWA of NREMS[16,21]. To verify the influence of $Na_v1.2$ N1467D mutation on the channel's slow inactivation,

we performed whole-cell patch-clamp recordings from layer 5 pyramidal neurons in both tamoxifen-induced *N1467D* and WT mice (Extended Data Fig. 2d, e). Compared to neurons from WT mice, those from *N1467D* mice manifested significant impairments in slow inactivation (Fig. 1e-h). Specifically, across a range of voltages, the sodium current in *N1467D* mice displayed reduced slow inactivation with delayed onset and accelerated recovery (Fig. 1f-h). Thus, the *Scn2a*$^{N1467D/fl}$*; CAGG*$^{Cre\text{-}ERTM/+}$ strain serves as a viable genetic model for dissecting the role of $Na_v1.2$ in sleep regulation.

The *N1467D* mice exhibited normal activity in EEG and electromyogram (EMG), as well as normal body weights (Extended Data Fig. 2c, f). Detailed examination of sleep and wakefulness behavior of *N1467D* mice showed that the transgenic mice exhibited a lower density of SWA during NREMS (Fig. 1i-k), suggesting that the baseline sleep need was decreased. Furthermore, the elevated NREMS SWA by 6 h sleep deprivation (SD6) in wild-type mice were completely diminished in *N1467D* mice (Fig. 1l, m). In addition, *N1467D* mice exhibited a normal wake and NREMS time, but shorter REMS time during the light phase and dysregulated REMS EEG spectral power in multiple frequency (Hz 1–9) (Extended Data Fig. 2g-s). These results, together with those of *N1467D/+* mice (Fig. 1k, m), suggest that $Na_v1.2$ regulates sleep need in an allele-dosage dependent manner.

To test whether $Na_v1.2$ also acts as a downstream effector of SLEEPY kinase, we expressed an active shorter version of SIK3 kinase (sSLP) by retro-orbital injection (ROI) with recombinant AAV-PHP.eB *Camk2a-HA-sSLP* virus in mouse brain excitatory neurons[22] (Fig. 1n-v and Extended Data Fig. 3a-h). By immunoblotting, we confirmed the robust sSLP expression and elevated phosphorylation of its substrates (Fig. 1o). Consistent with previous reports[23], forced expression of sSLP causes shorter wake time, increased NREMS, and elevated EEG delta power during NREMS, REMS and wakefulness in wild-type mice (Fig. 1p, r, t and Extended Data Fig. 3a-c). Notably, all these phenotypes are fully rescued in *N1467D* mice (Fig. 1q, s, t and Extended Data Fig. 3e-g). Similarly, elevated SWA and time of NREMS by 6 h sleep deprivation in sSLP expressed wild-type mice were also diminished in *N1467D* mice

(Fig. 1u, v and Extended Data Fig. 3d, h), suggesting that $Na_v1.2$ regulates sleep downstream of SLEEPY kinase.

The sleep-regulated phosphorylation-patch of $Na_v1.2$ consists of 27 phosphopeptides (28 phosphorylation sites), among which 19 phosphopeptides (20 phosphorylation sites) are up-regulated in the *Sleepy* or sleep-deprived models (Extended Data Fig. 4a-c, Supplementary Table 3). Kinase motif-enrichment analysis[24] identified 5 sites as PKA substrate sites and 2 as PKC sites (Extended Data Fig. 4d, and Supplementary Table 4). This finding was further corroborated by immunoprecipitation of the endogenous $Na_v1.2$ protein under the conditions of 6 h of ad libitum sleep (S6) and sleep deprivation (SD6) (Fig. 2a, b). Moreover, we discovered that the endogenous $Na_v1.2$ protein interacts with the A-kinase anchoring protein AKAP 7 (Fig. 2c, d), and this interaction might mediate the phosphorylation and slow inactivation transition of $Na_v1.2$ by PKA[18,19,25,26]. To test this, we employed a Stapled AKAP Disruptor Peptide (STAD-2) to specifically disrupt the interaction between PKA and AKAP 7 proteins by intracerebroventricular injection (Fig. 2c).

The administration of STAD-2 significantly suppressed the phosphorylation status (Fig. 2d), and the slow inactivation of $Na_v1.2$, as manifested by changes in voltage dependence, onset and recovery, reminiscent of those observed in *N1467D* mice (Fig. 2e-h, Extended Data Fig. 4e). Consistent with this, the STAD-2 treatment significantly decreased the baseline and rebound SWA after 6 h of sleep deprivation, but not duration, of NREMS (Fig. 2i-m, and Extended Data Fig. 4f-o). Additionally, the lower-frequency power in EEG was also reduced during REMS and wakefulness in the STAD-2 treated mice (Extended Data Fig. 4p-s), which might be attributed to other PKA substrates[27]. Furthermore, the STAD-2 treatment also led to a significant reduction of REMS duration as seen in *N1467D* mutant mice (Extended Data Fig. 2s and 4s). Collectively, these results suggest that the PKA/AKAP 7-mediated phosphorylation of $Na_v1.2$ may play a critical role in sleep regulation.

Sleep and wakefulness can induce global phosphorylation alterations in the brain proteome[8-10,12]. In turn, some of these changes are closely related to the regulation of sleep homeostasis[12]. To investigate the impacts of $Scn2a^{N1467D}$ on the sleep

phosphoproteome, we performed quantitative proteomic and phosphoproteomic analyses of brains lysates from wild-type and *N1467D* mice in S6 and SD6 conditions (Fig. 3a and Supplementary Table 5). The brain proteomic analysis quantified 12,341 proteins, very few proteins showed significant changes in abundance ($P < 0.01$) in the comparisons between *N1467D* and WT samples in either S6 or SD6 conditions, SD6 and S6 samples from *N1467D* or WT mice, respectively (Fig. 3b and c, Extended Data Fig. 5a and b). The amount of $Na_v1.2$ proteins was specifically reduced by ~70% in *N1467D* relative to WT samples, which was in line with the immunoblotting results (Fig. 1d and 3d).

Phosphoproteomic analyses quantified 35,246 phosphopeptides (Fig. 3e and f, Extended Data Fig. 5c and d). The brain phosphoproteomes of WT mice showed significant changes ($P < 0.02$) in SD6/S6 (6.2%) comparison (Fig. 3e). However, such alterations were suppressed in *N1467D* samples to a great extent (0.91%) (Fig. 3f). Notably, both ΔPs analysis[12] and kinase motif-enrichment analysis[28] also found that the cumulative phosphorylation of SNIPPs and the up-regulated intracellular signalling pathways involved in sleep regulation (SRKs, sleep related kinases), which were induced by sleep deprivation in WT mice, were completely abolished in *N1467D* mice (Fig. 3g-j). These results were precisely in line with the absence of rebound SWA following sleep deprivation (Fig. 1l, m).

Although N1467D mutation of $Na_v1.2$ also causes brain phosphoproteome changes in S6 (3.2%) or SD6 (2.3%) conditions (Extended Data Fig. 5c-d), only few SNIPPs and sleep signalling pathways were altered (Extended Data Fig 5e-h). Furthermore, we found the phosphorylation status of multiple PKA sites within the sleep regulated phosphorylation-patch are significantly increased in *N1467D* samples at S6（*N1467D*/WT） condition, which indicates a feedback regulation of PKA-$Na_v1.2$ pathway in the reduced sleep need *N1467D* mice (Fig. 3k, Extended Data Fig. 6). The fact that *N1467D* mice exhibit a lower basal SWA suggests that the attenuation of slow inactivation resulting from the N1467D mutation serves as the downstream factor in controlling the basal sleep need (Fig. 1i, m).

Moreover, behavioral tests, including the novel object recognition (NOR) and Morris water maze (MWM), demonstrated that the short-term learning ability and spatial memory were markedly impaired (Fig. 3l-t). Mechanistically, this impairment might be associated with the deficiency of normal sleep in *N1467D* mice. Taken together, these observations imply that $Na_v1.2$ is not only regulated by sleep, but also gates other sleep-associated signalling pathways and molecular substrates to control sleep need and sleep related behaviors.

$Na_v1.2$, an AIS sodium channel, plays a pivotal role in action potential initiation and backpropagation as well as neuronal excitability[14,29]. Mutations within the *Scn2a* gene have been linked to a variety of neuropsychiatric disorders, including autism and epilepsy. Moreover, numerous patients carrying these mutations frequently encounter sleep disturbances[30-32]. This study elaborates on the physiological role of $Na_v1.2$ in the regulation of sleep homeostasis through a specific regulatory mechanism that involves phosphorylation and the electrophysiological properties of the channel. The detailed information obtained from this study may present an opportunity to identify signaling pathways that can be manipulated pharmacologically to alleviate various sleep and psychological disorders, such as depression[33,34].

Acknowledgements We thank Drs. Masashi Yanagisawa and Hiromasa Funato for sleep analysis software; the core facilities of HIT Center for Life Science for technical assistances. This work was supported by grants from the National Major Project of China Science and Technology Innovation 2030 for Brain Science and Brain-Inspired Technology (2021ZD0203402 to Z.W.), the National Natural Science Foundation of China (32071011 to Z.W.), the China National Key R&D Program (2022YFA1604502 to Z.W. and G.W.), the Lingang Laboratory & National Key Laboratory of Human Factors Engineering Joint Grant (LG-TKN-202203-01 to Z.W.), Frontiers Science Center for Matter Behave in Space Environment to Z.W., the National Natural Science Foundation of China (31970912 to G.W.), the Fundamental Research Funds for the Central Universities (HIT.DZJJ.2023132 to J.L.) and the startup funds from the HIT Center for Life Science.

Author Contributions Z.W. and Y.L. conceived and designed the experiments. Y.L. and J.M. completed sleep experiments. Y.L., J.M. and C.Z. completed mass spectrometric experiments. K.Y. and G.W. completed electrophysiological experiments. Y.L., H.T. and Q.S. completed all other experiments. Y.L., J.L., J.M. and Z.W. analyzed the data and made the figures. Z.W. and Y.L. wrote the manuscript with inputs from all other authors.

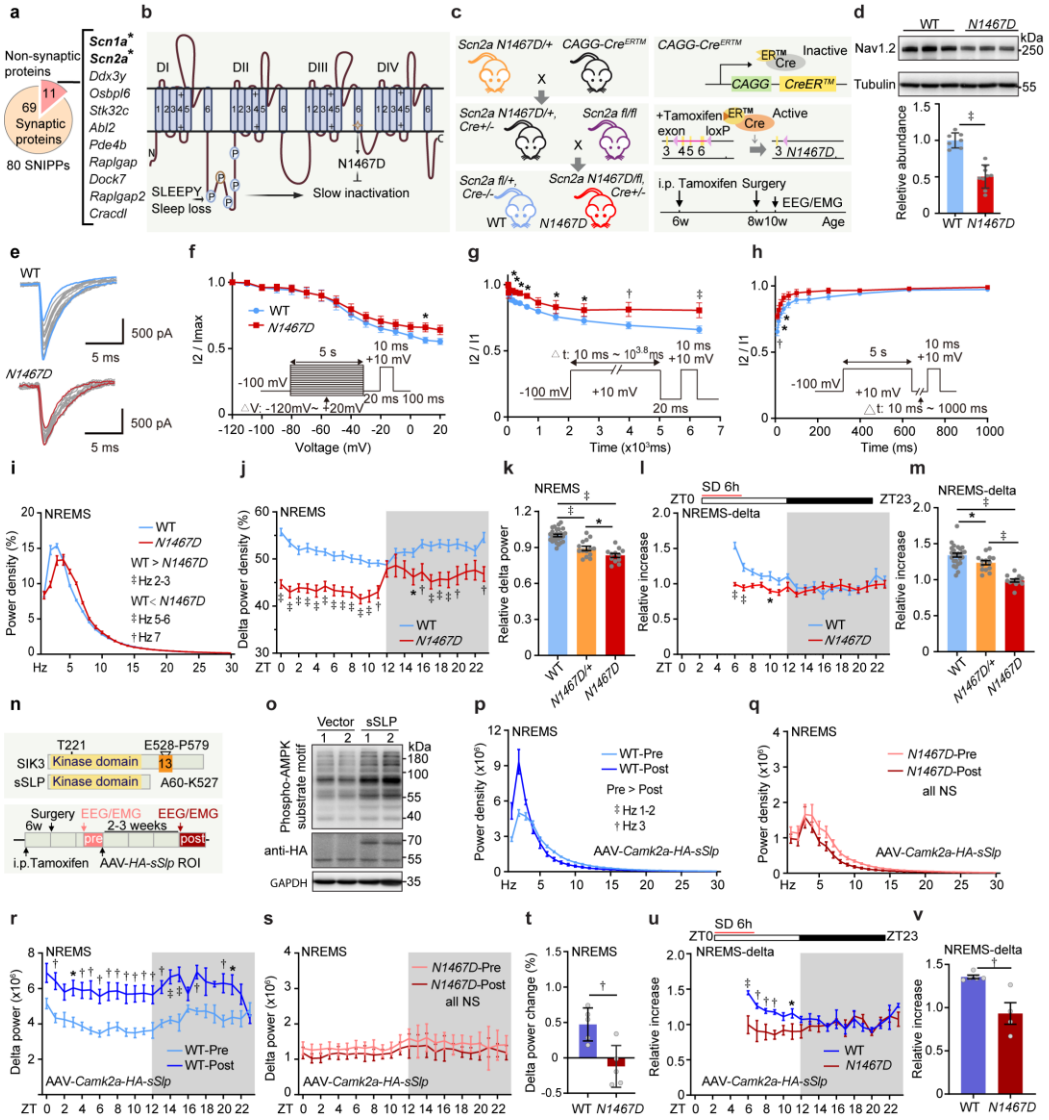

Fig. 1. Impaired slow inactivation of $Na_v1.2$ attenuates SWA of NREMS.

(a) Non-synaptic proteins among the 80 SNIPPs proteins. Stars, AIS proteins.

(b) The structure of $Na_v1.2$ includes four homologous transmembrane domains (DI, DII, DIII, DIV) and three intracellular loops (DI-II, DII-III, DIII-IV). Each domain consists of six transmembrane helices (S1-S6). SLEEPY and sleep deprivation increase the phosphorylation level in the DI-II loop, which promotes slow inactivation. The slow inactivation is impaired by N1467D mutation in the DIII-S6 linker region.

(c) Schematic of constructs for tamoxifen-inducible *Scn2a*^{N1467D}*(N1467D)* homozygous mice and experimental protocol.

(d) Immunoblotting (top) and quantification (bottom) of $Na_v1.2$ in brain lysates from tamoxifen-injected WT (n=7) and *N1467D* mice (n=9).

(e-h) Measurements of slow inactivation for WT (n=17) and *N1467D* (n=16) mice.

Representative current traces (e), voltage dependence (f) and onset (g) of slow inactivation, and recovery (h) from slow inactivation. The insets in (f-h) display voltage protocols.

(i-m) Sleep analyses for wild-type and *N1467D* mice. Relative EEG power spectra during NREMS (ZT0-23) (i), 24-h (j) and mean (k) NREMS delta power (ZT0-11), changes in NREMS delta power after 6 h sleep deprivation relative to baseline at each ZT (l) and mean (m) increase (ZT6-8) for WT (n=12), *N1467D*/+(n=14) and *N1467D* (n=12).

(n) Schematic diagram of the protein structure of truncated SIK3 protein (sSLP) for retro-orbitally injected (ROI) AAV expression, and the experimental design for EEG/EMG recording.

(o) Immunoblotting of brain lysates from mice injected with AAV expressing HA-sSLP with AMPK phosphorylation substrate motif antibody.

(p-v) Sleep analyses for both WT mice (n=5) and *N1467D* mice (n=5) injected with AAV-*Camk2a-HA-sSlp*. Absolute EEG power spectra during NREMS (ZT0-23) (p, q), 24-h absolute NREMS delta power (r, s) and relative NREMS delta power changes (t) at baseline before (pre) and after (post) virus injection. NREMS delta power changes following 6 h sleep deprivation relative to baseline at each ZT (l) and mean (m) increase (ZT6-8). Data shown as mean ± SD (d, t) or mean ± s.e.m. (f-m, p-s, u-v), two-way ANOVA with Sidak's test (i-j, l, p-s); two-way ANOVA with Fisher's LSD test (f-h, u); two-tailed unpaired *t*-test (d, k, m, t, v). * $P < 0.05$; † $P < 0.01$; ‡ $P < 0.001$; NS, not significant, $P > 0.05$.

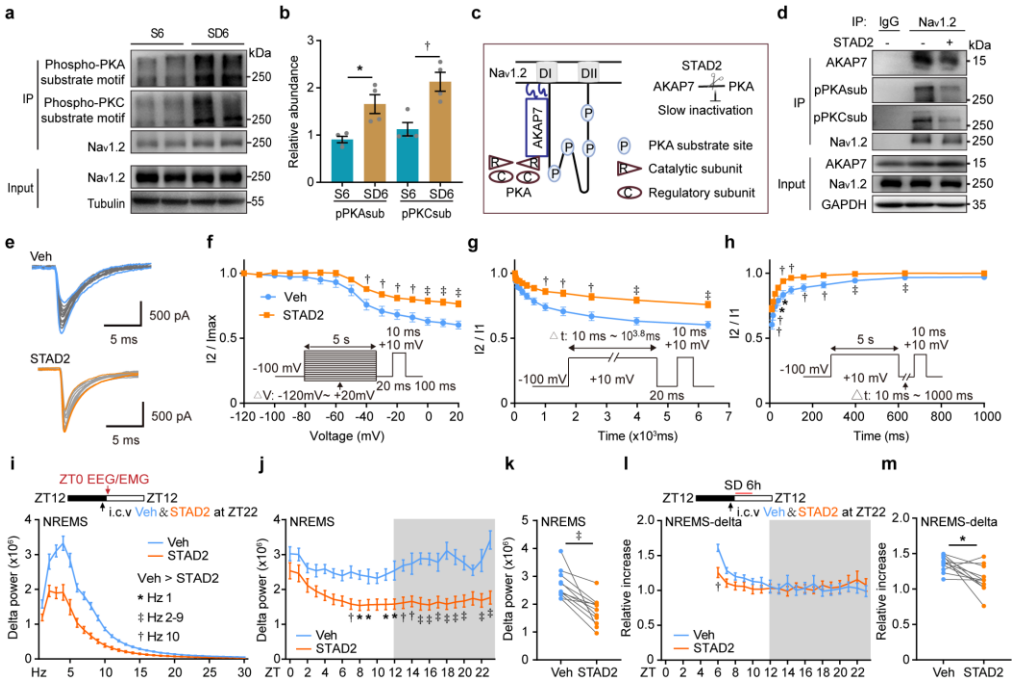

Fig.2. PKA mediated slow inactivation is required for homeostatic sleep response.

(a-b) Phosphorylation levels of the PKA substrate motif and PKC substrate motif in $Na_v1.2$ immunoprecipitates under S6 and SD6 conditions (a), and corresponding quantification (b) (n = 4).

(c) Schematic of the interaction between PKA, AKAP7 and the linker region (DI–II) of $Na_v1.2$. STAD2 disrupts the interaction between AKAP7 and PKA.

(d) Immunoprecipitation confirms the interaction between $Na_v1.2$ and AKAP7.

(e-h) Measurements of slow inactivation for mice intraventricular injected with vehicle (Veh) (n=16) and STAD2 (n=21). Representative current traces (e), voltage dependence (f) and onset (g) of slow inactivation, and recovery (h) from slow inactivation. The insets in (f-h) display voltage protocols.

(i-m) Sleep analyses for C57/B6J (n=11) intraventricular injected with Veh or STAD2 at ZT22. Absolute EEG power spectra during NREMS (ZT0-23) (i), 24-h (j) and mean absolute delta power of NREMS (ZT0-23) (k), NREMS delta power changes following 6 h sleep deprivation relative to baseline at each ZT and mean (m) increase (ZT6-8). Data shown as mean ± s.e.m. (b, f-j, l), two-way ANOVA with Fisher's LSD test (f-h); two-way ANOVA with Sidak's test (i-j, l); two-tailed unpaired *t*-test (b);

two-tailed paired *t*-test (k, m). * $P < 0.05$; † $P < 0.01$; ‡ $P < 0.001$; NS, not significant, $P > 0.05$.

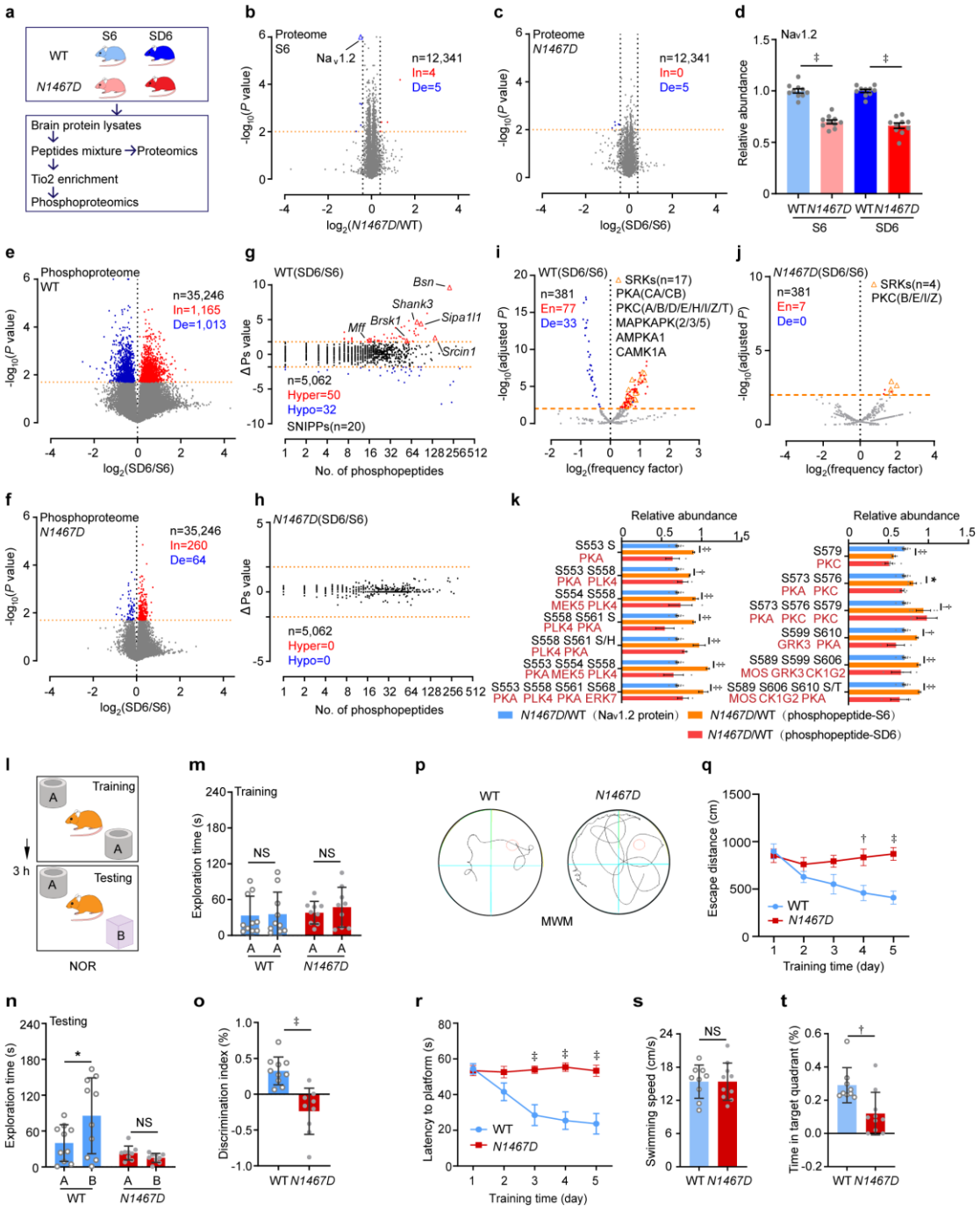

Fig.3. Na$_v$1.2 controls phosphorylation state of brain proteome and learning behaviors.

(a) Experimental approach for proteomic and phosphoproteomic profiling across four models.

(b-f) Volcano plots illustrating the changes in proteins (b, c) in S6 (*N1467D*/WT) and *N1467D* (SD6/S6) comparisons and in phosphopeptides (e, f) in WT (SD6/S6) and *N1467D* (SD6/S6) comparisons, and abundance analysis of Na$_v$1.2 protein. Multiple unpaired t-test (*P* value) (b, c, e, f). In, increased; De, decreased.

(g-j) Global ΔPs analysis of phosphoproteins in WT (SD6/S6) (g) and *N1467D* (SD6/S6) (h) comparisons. The number of hyperphosphorylated (Hyper) and hypophosphorylated (Hypo) proteins are shown. Dashed line represents ΔPs = ±1.8. Kinase motif enrichment analysis of phosphoproteomics data in WT (SD6/S6) (i) and *N1467D* (SD6/S6) (j) comparisons. SRKs, sleep related kinases. Dashed line represents-$\log_{10}$(adjusted *P*) =2. En, enriched; De, depleted.

(k) Phosphopeptides located in DI-II that show significant differences compared to the relative abundance of the $Na_v1.2$ proteome, along with the predicted kinases for these sites. Red represents sleep-related kinases.

(l-o) Schematic of the novel object recognition (NOR) experimental protocol (l). Exploration time during the training phase (m), testing phase (n) and discrimination index (o) for WT (n=10) and *N1467D* mice (n=9).

(p-t) The swimming trajectory on the fifth day of the Morris water maze (MWM) task (p), escape distance (q) and latency (r), swimming speed (s) and the ratio of time in target zone (t) on the sixth day for WT (n=9) and *N1467D* (n=10). Data shown as mean ± SD (m-o, s-t) or mean ± s.e.m. (d, k, q, r), two-way ANOVA with Sidak's test (q, r); two-tailed unpaired *t*-test (m-o, s, t). * $P < 0.05$; † $P < 0.01$; ‡ $P < 0.001$; NS, not significant, $P > 0.05$.

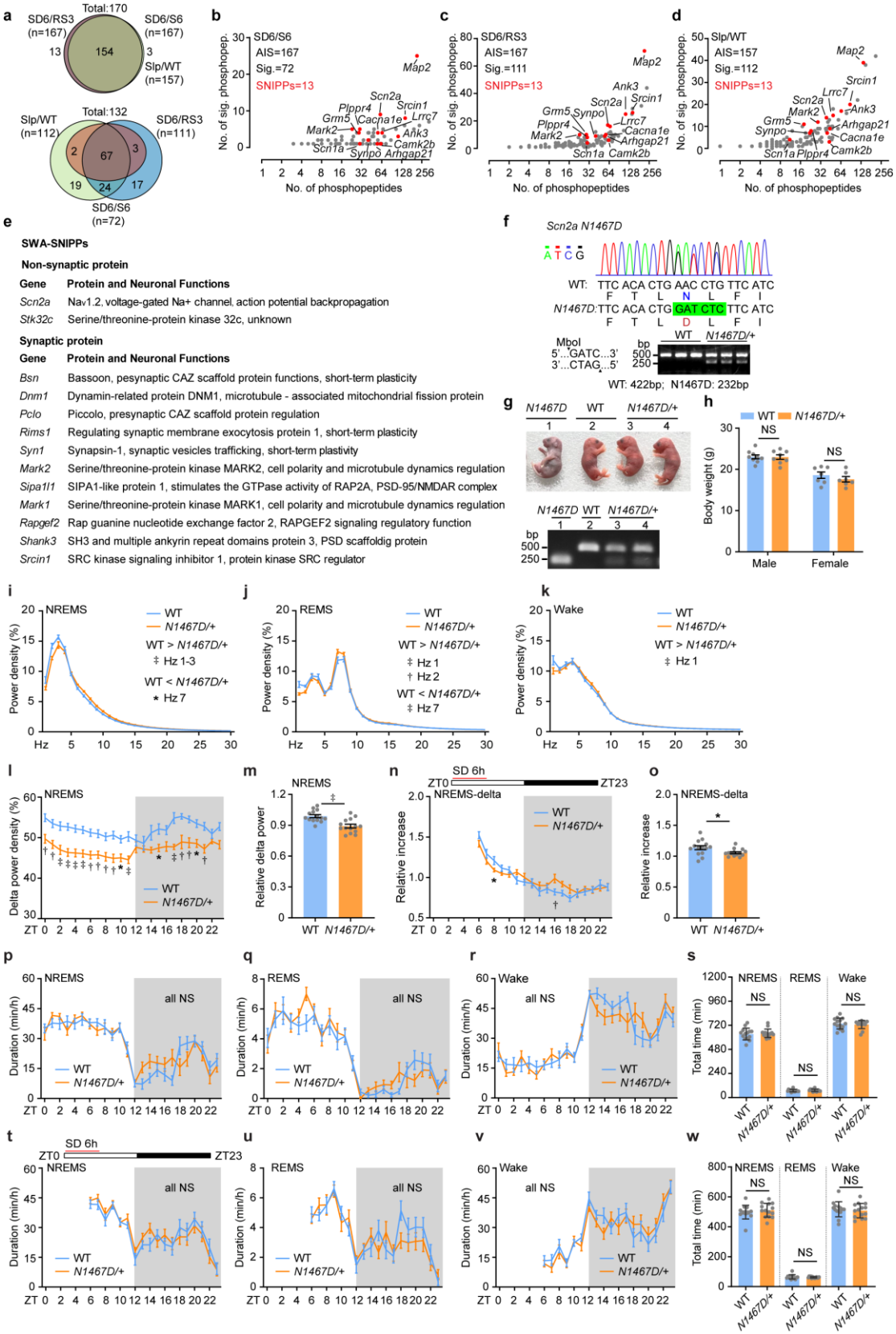

Extended Data Fig. 1. Generation and characterization of *Scn2a*^{N1467D} mutant mice.

(a) Venn diagrams of quantified axon initial segment (AIS) proteins (top) and AIS proteins with significantly changed phosphopeptides (bottom) among three groups, the protein number in each group are shown in parentheses.

(b-d) The number of quantified and significant changed phosphopeptides of AIS proteins across the three experimental groups. Red dots indicate SNIPPs proteins.

(e) Summary of the information and functions of the 13 SWA-SNIPPs.

(f) Direct sequencing, genotyping designs, and RT-PCR of the *N1467D/+* mutant mouse.

(g) Postnatal mortality of *N1467D* mice and genotyping results.

(h) Comparison of body weight between WT (n=9 male, 7 female) and *N1467D/+* (n= 8 male, 7 female) mice.

(i-w) Sleep analyses for WT (n=14) and *N1467D/+*(n=14). Relative EEG power spectra (i-k), 24-h (i) and mean (m) NREMS delta power (ZT0-11), changes in NREMS delta power after 6 h sleep deprivation relative to baseline at each ZT (n) and mean (o) increase (ZT8-10), hourly time (p-r) and total time at baseline (s), hourly time (t-v) and total time (w) after SD6. Data shown as mean ± SD (s, w) or mean ± s.e.m. (h-r, t-v), two-way ANOVA with Sidak's test (i-k, l, p-r, t-v), two-way ANOVA with Fisher's LSD test (n), two-tailed unpaired *t*-test (h, m, o, s, w). * $P < 0.05$; † $P < 0.01$; ‡ $P < 0.001$; NS, not significant, $P > 0.05$.

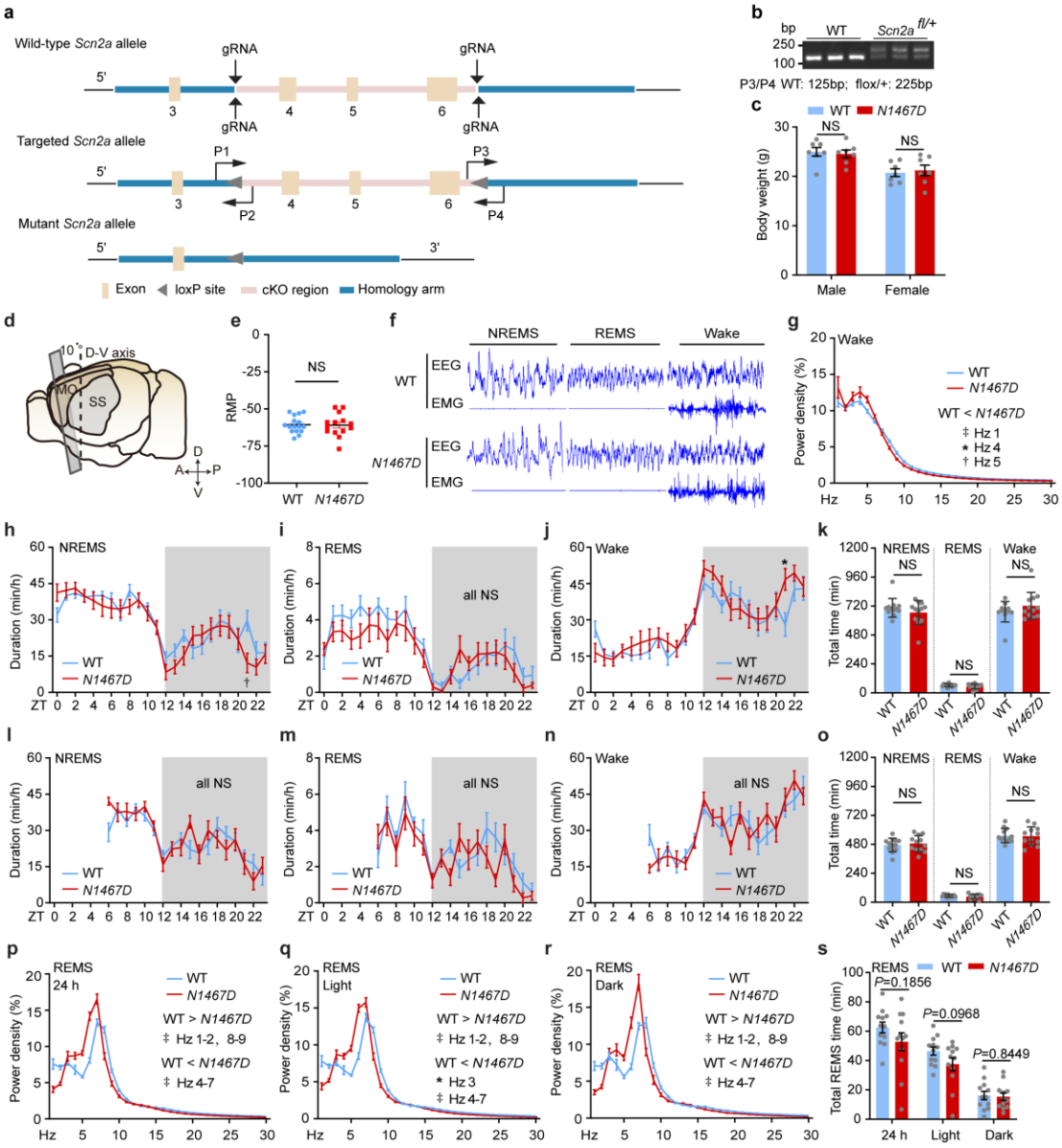

Extended Data Fig. 2. Sleep analysis of *N1467D* mice.

(a-c) Design strategy (a), genotyping (b) and body weight comparison (c) for WT (n=7 male, 7 female) and *N1467D*/+ (n=7 male, 7 female) mice.

(d) Schematic of brain slice sampling. Slicing plane is tilted forward by 10°. MO, the motor cortex; SS, the somatosensory cortex.

(e) Comparison of resting membrane potential (RMP) of neurons from WT (n=16) and *N1467D* (n=14) mice.

(f) Representative 4-s EEG and EMG for NREMS, REMS and wake for WT mice or *N1467D* mice.

(g-s) Sleep analyses for WT (n=12) and *N1467D* (n=12) mice. Relative EEG power

spectra during wake (ZT0-23) (g), hourly time (h-j) and total time at baseline (k), hourly time (l-n) and total time after SD6 (o), relative EEG power spectra during REMS (p-r) and total REMS time at baseline (s). Data shown as mean ± SD (k, o) or mean ± s.e.m. (c, e, g-j, l-n, p-s), two-way ANOVA with Sidak's test (g-j, l-n, p-r) or unpaired *t*-test (c, e, k, o, s). * $P < 0.05$; † $P < 0.01$; ‡ $P < 0.001$; NS, not significant, $P > 0.05$.

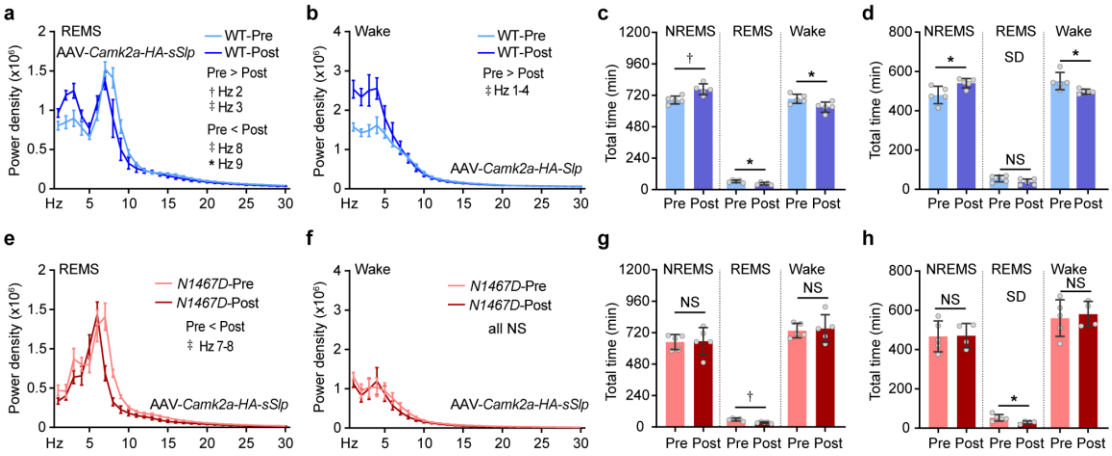

Extended Data Fig. 3. $Na_v1.2$ is downstream of SIK3 kinase in the regulation of sleep.

(a-h) Sleep analyses for both WT mice (n=5) and *N1467D* mice (n=5) injected with AAV-*Camk2a-HA-sSlp*. Relative EEG power spectra during REMS and wake before (pre) and after (post) virus injection (a, b), total time at baseline (c) and total time after SD6 (d) for WT mice. Relative EEG power spectra before (pre) and after (post) virus injection (e, f), total time at baseline (g) and total time after SD6 (h) for *N1467D* mice. Data shown as mean ± SD (c-d, g-h) or mean ± s.e.m. (a-b, e-f), two-way ANOVA with Sidak's test (a, b, e, f) or unpaired *t*-test (c, d, g, h). * $P < 0.05$; † $P < 0.01$; ‡ $P < 0.001$; NS, not significant, $P > 0.05$.

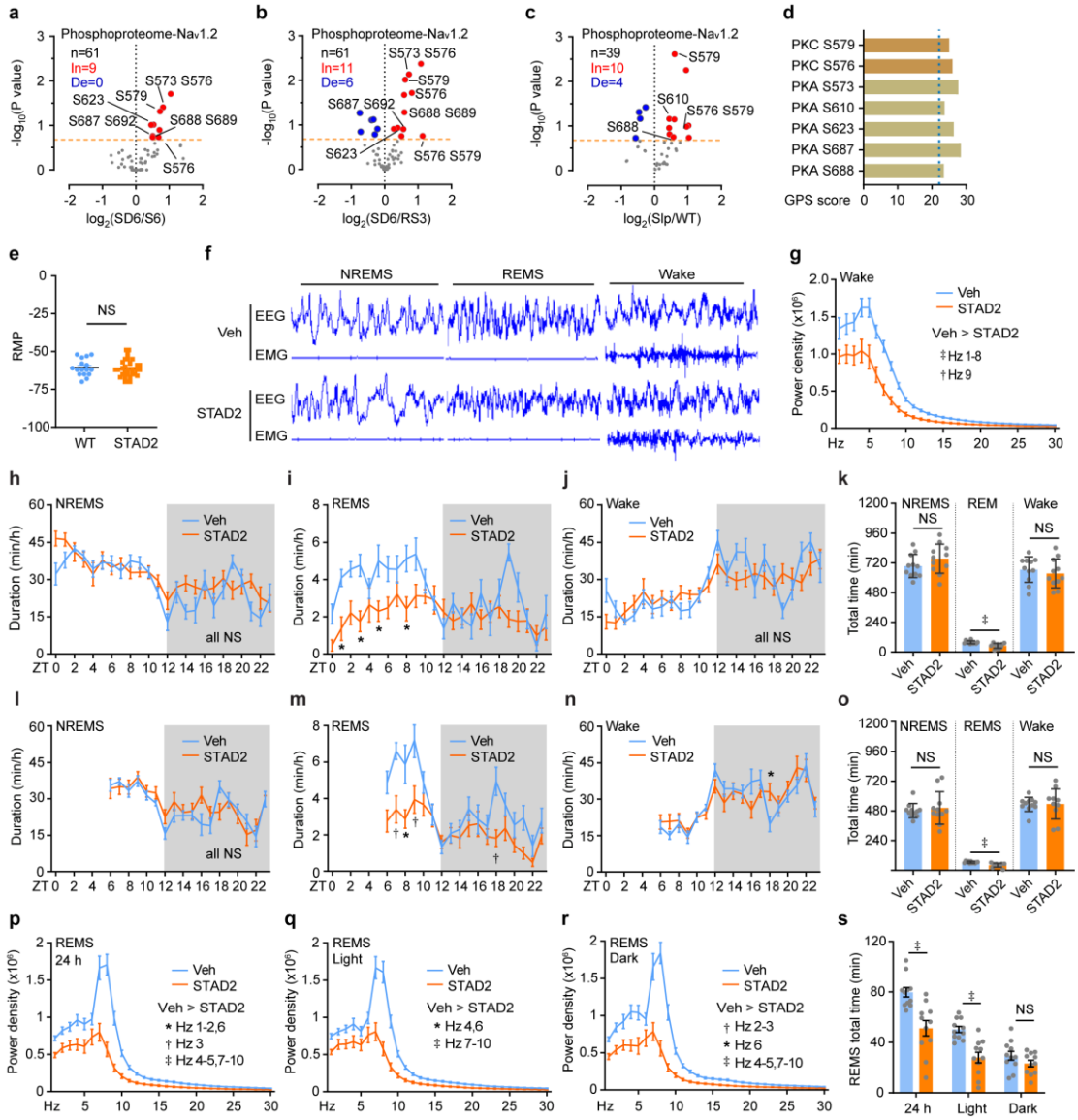

Extended Data Fig. 4. Inhibition of the interaction between PKA and AKAP7 reduces EEG power and REMS time.

(a-d) Volcano plots illustrating the changes in phosphopeptides of $Na_v1.2$ detected in SD6/S6 (a), SD6/RS3 (b) and Sleepy/WT (c) comparisons. The predicted PKA and PKC sites are shown (d), with blue dashed lines indicating GPS score as 22.8. GPS, Group-based Prediction System. In, increased; De, decreased.

(e) Comparison of resting membrane potential (RMP) of neurons from Veh (n=16) or STAD2-treated (n=30) mice.

(f) Representative 4-s EEG and EMG for NREMS, REMS and wake for Veh or STAD2-treated mice.

(g-s) Sleep analyses for C57/B6J (n=11) intraventricular injected with Veh or STAD2

363 at ZT22. Absolute EEG power spectra during wake (g), hourly time (h-j) and total
364 time at baseline (k), hourly time (l-n) and total time after SD6 (o), absolute EEG
365 power spectra analysis of REMS (p-r) and total REMS time at baseline (s). Data
366 shown as mean ± SD (k, o) or mean ± s.e.m. (e, g-j, l-n, p-s), two-way ANOVA with
367 Sidak's test (g-j, l-n, p-r) or unpaired *t*-test (e, k, o, s). * $P < 0.05$; † $P < 0.01$; ‡ $P <$
368 0.001; NS, not significant, $P > 0.05$.
369

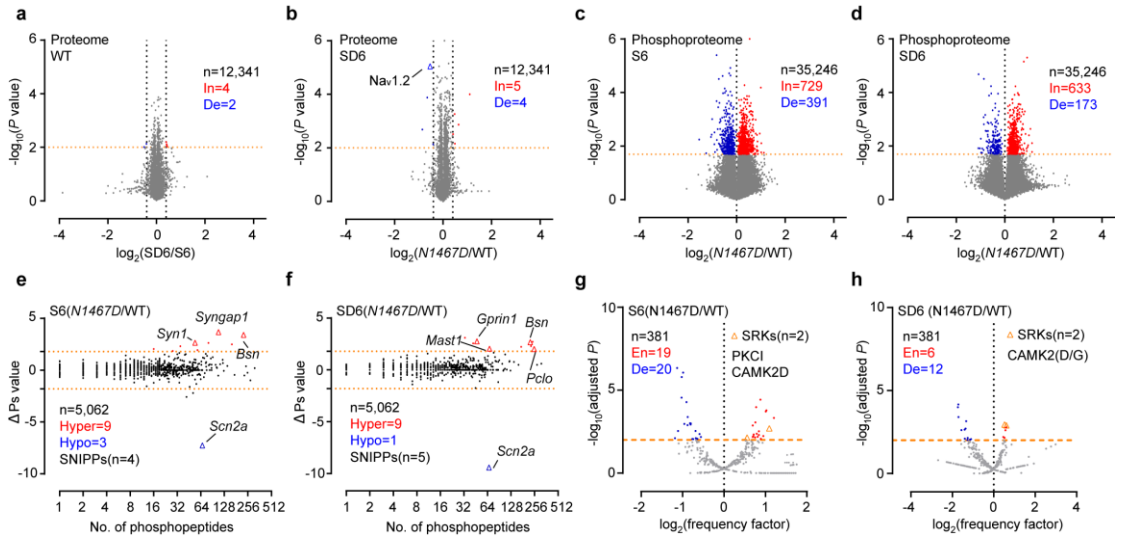

Extended Data Fig. 5. Brain phosphoproteome analysis of *N1467D* mice.

(a-d) Volcano plots illustrating the changes in proteins (a, b) in WT (SD6/S6) and SD6 (*N1467D*/WT) comparisons and in phosphopeptides (c, d) in S6 (*N1467D*/WT) and SD6 (*N1467D*/WT) comparisons. Multiple unpaired *t*-test (*P* value). In, increased; De, decreased.

(e-h) Global ΔPs analysis of phosphoproteins in S6 (*N1467D*/WT) and SD6 (*N1467D*/WT) comparisons (e, f). The number of hyperphosphorylated (Hyper) and hypophosphorylated (Hypo) proteins are shown in each comparison. Dashed line represents ΔPs = ±1.8. Kinase motif enrichment analysis of phosphoproteomics data in S6 (*N1467D*/WT) and SD6 *(N1467D*/WT) comparisons (g, h). SRKs, sleep related kinases. Dashed line represents -log10(adjusted *P*) =2. En, enriched; De, depleted.

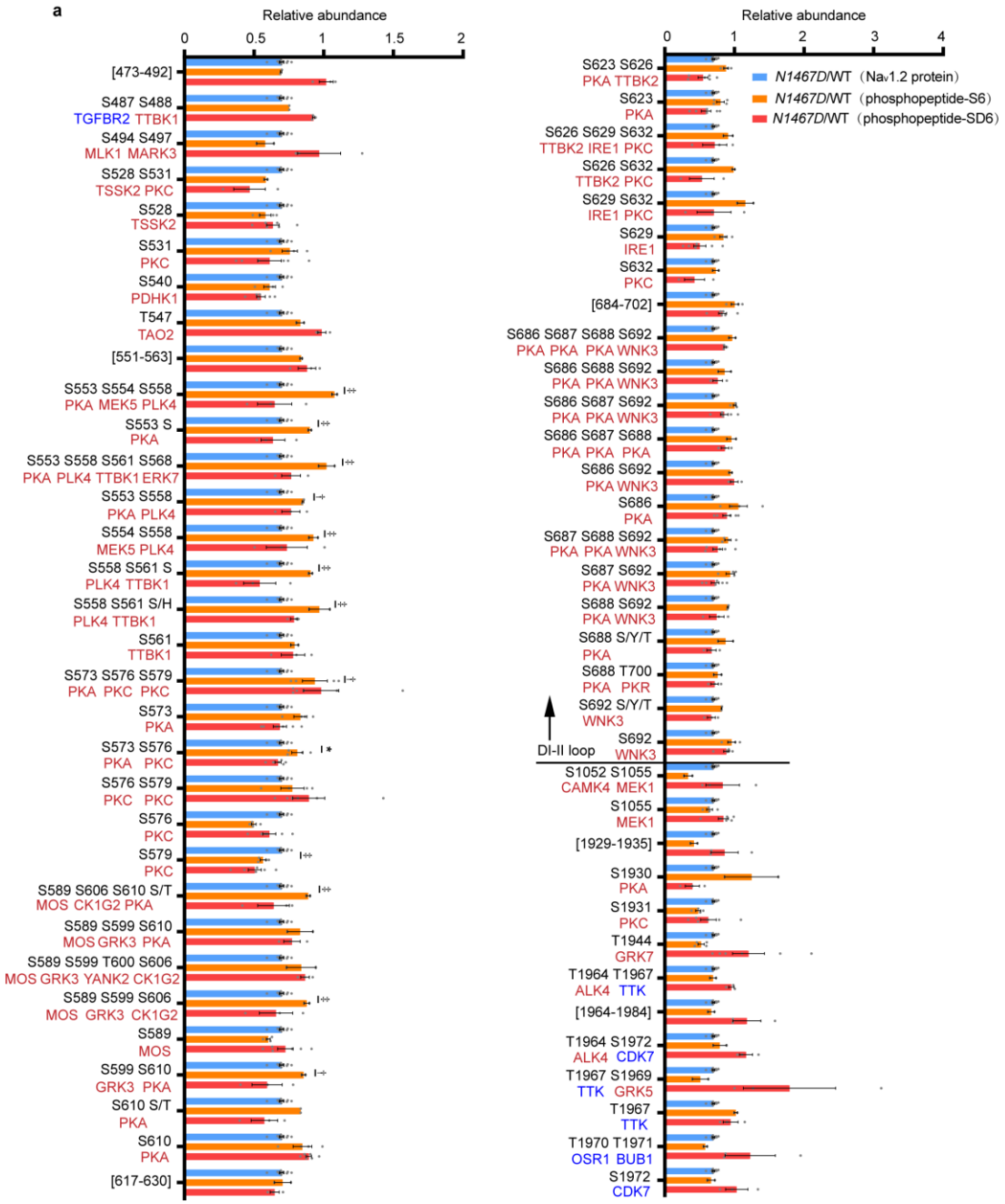

Extended Data Fig. 6. The quantified phosphopeptides of $Na_v1.2$ are clustered in DI-II loop.

(a) A summary of all quantified phosphopeptides of $Na_v1.2$ under S6 (*N1467D*/WT-S6) and SD6 (*N1467D*/WT-SD6) conditions and compared to the relative abundance of the $Na_v1.2$ proteome (*N1467D*/WT-$Na_v1.2$ protein), along with the predicted kinases for these sites. Red represents sleep-related kinases, while blue represents non-sleep-related kinases. Mean ± s.e.m., Multiple *t* tests. * $P < 0.05$; † $P < 0.01$; ‡ $P < 0.001$.

Materials and Methods

Animals.

All animal experiments were conducted following procedures approved by the Harbin Institutional Animal Care and Use Committee of Harbin Institute of Technology (HIT/IACUC). The mice were housed under appropriate temperature and humidity conditions, with a 12-hour light-dark cycle. All mice were the C57BL/6J strain background, provided with adequate food and water, and housed until 8 to 12 weeks for experimentation. Point mutation mice *Scn2a*^{N1467D} and, *Scn2a*^{flox} mice and *CAGG*$^{Cre\text{-}ERTM/+}$ mice were purchased from Cyagen Bioscience (Guangzhou, China). We crossed *CAGG*$^{Cre\text{-}ERTM/+}$ mice with *Scn2a*$^{N1467D/+}$ mice to obtain *Scn2a*$^{N1467D/+,\ Cre+/-}$, and then crossed with *Scn2a*$^{fl/fl}$ mice to obtain *Scn2a*$^{N1467D/fl,\ Cre+/-}$ mice.

Tamoxifen supplementation.

Tamoxifen (S1238, Selleck) was dissolved in corn oil to prepare a solution with a concentration of 20 mg/ml. When the mice reached 6 weeks, tamoxifen was intraperitoneally administered at a dose of 75 mg/kg to *Scn2a*$^{N1467D/fl,\ Cre/+}$ mice and their littermate *Scn2a*$^{fl/+}$ mice for five consecutive days. It was observed that tamoxifen administration did not have an impact on the body weight of the mice.

EEG recording and sleep phenotype analysis.

The EEG recordings and sleep phenotype analysis were carried out as previously described[1,12,35]. All the mice that underwent EEG recording were male and at least 8 weeks. During the implantation of EEG electrodes, the mice were kept under continuous anesthesia with isoflurane. Their heads were fixed in a stereotaxic frame to ensure a horizontal orientation. The fur covering the skull was shaved off, and the surface of the skull was disinfected using hydrogen peroxide. Lambda (0, 0, 0) was marked as the origin with a marker pen. With a handheld drill, four holes were drilled in the mouse skull at the coordinates (-1.27, 0, 0), (-1.27, 5.03, 0), (1.27, 5.03, 0), and (1.27, 0, 0). The EEG electrodes were inserted to a depth of 1 mm at these positions and then secured to the skull with dental cement (3M). Subsequently, the scalp was sutured. Following the surgical procedure, the mice were housed individually and allowed to recover for 7 days. After that, they were connected to recording cables and

given an additional 7 days for habituation. The EEG/EMG recording started 14 days after the surgery and lasted for 4 consecutive days.

Sleep deprivation was carried out on the fourth day starting from Zeitgeber Time 0 (ZT0). Mice were placed on a rocking platform rotating at 190 revolutions per minute (rpm), and gentle handling was applied as necessary until ZT6. The EEG/EMG data were first analyzed semi-automatically and then manually corrected to ensure accuracy. The Fast Fourier transform was applied to the EEG data within the frequency range of 1 to 30 Hz and in 20-second epochs. The waking state was defined as featuring low-amplitude, fast EEG coupled with high-amplitude, variable EMG. NREMS was characterized by high-amplitude, delta (Hz 1-4) frequency EEG accompanied by low muscle tone. REMS was characterized by dominant theta (Hz 6-9) frequency EEG along with muscle atonia. Absolute and relative power spectrum analyses were performed for each ZT period. The relative power spectrum (%) was calculated by expressing the EEG power in each frequency band as a percentage of the total power across all frequency bands (Hz 1-30). The duration and power density of NREMS, REMS, and the waking state were averaged on an hourly basis from ZT0 to ZT23. During data analysis, researchers were kept unaware of the genotype of the mice to ensure objectivity. Meanwhile, animals with unreadable EEG signals were excluded from the study to maintain data quality.

Immunoprecipitation and immunoblotting.

Immunoprecipitation analysis was performed following the standard protocol with minor modifications[12]. Brain tissue was promptly excised from the mice, placed into cryopreservation tubes, and then stored in liquid nitrogen before being transferred to -80°C freezer. Both the glass homogenizers and the brain tissue lysis buffer were pre-cooled during the immunoprecipitation process. The lysis buffer consisted of 1% Triton X-100, 150 mM NaCl, 20 mM HEPES (pH 7.4), 2 mM $MgCl_2$, 1 mM EDTA, 15 mM NaF, 20 μM Leupeptin hemisulfate, 10 μM Pepstatin A, 1 mM PMSF, 100 mM Sodium orthovanadate, 4 mM Sodium tartrate dibasic dihydrate, and a protease-phosphatase inhibitor cocktail. The brain tissue was placed in a glass homogenizer, 4 ml of lysis buffer was added, along with nuclease (Thermo).

Homogenization was performed at 4°C. After lysis, the samples were incubated on ice for 30 minutes, after which the supernatant was collected and centrifuged at 13,000 g for 20 minutes at 4°C. The resulting supernatant was then subjected to BCA protein concentration assay. For immunoprecipitation, 35 mg of protein was mixed with 30 µl of Protein A/G PLUS-Agarose (sc-2003, Santa Cruz) and pre-incubated at 4°C for 30 minutes. The mixture was then centrifuged at 2,500 rpm for 5 minutes at 4°C, and the supernatant was collected. To the supernatant, 5 µl of anti-SCN2A ($Na_v1.2$) (#ASC-002, Alomone Labs) was added and incubated at 4°C for 1 h. Subsequently, 30 µl of Protein A/G PLUS-Agarose was added and incubated overnight at 4°C to isolate the immune complexes. Protein samples were separated and analyzed by SDS-polyacrylamide gel electrophoresis (PAGE) followed by Western blotting.

Immunoblotting was performed using the corresponding antibodies according to standard procedures. Antibodies utilized in this study encompassed anti-SCN2A($Na_v1.2$) (1:1000, #ASC-002, allomone labs), anti-β-Tubulin (9F3) (1：1000, #2128, Cell Signaling), anti-GAPDH (14C10) (1：1000, #2118, Cell Signaling), guinea pig anti-SCN2A($Na_v1.2$) (1:1000,ASC-002-GP, allomone labs), anti-phospho-PKC substrate motif ((K/R)XS*X(K/R)) (1:1000, #6967, Cell Signaling), anti-phospho-AMPK Substrate Motif (LXRXX(S*/T*) (1:1000, #5759, Cell Signaling), anti-phospho-PKA Substrate (RRXS*/T*) (1:1000, #9624, Cell Signaling), anti-HA (C29F4) (1:1000, #3724, Cell Signaling) and anti-AKAP7 (1:1000, 12591-1-AP, Proteintech).

Brain slice preparation and electrophysiology.

The preparation of motor cortical slices for electrophysiological recordings followed protocols established in previous studies[36,37]. Whole-cell patch-clamp recordings were conducted at 32-34°C using Model 2400 amplifiers (A-M Systems). The data were analyzed using Igor Pro 6 (WaveMetrics). All brain slices were obtained from 8-weeks mice. After decapitation, brain tissue was quickly extracted and immersed in ice-cold (0–4°C) artificial cerebrospinal fluid (ACSF) solution. The ACSF (pH 7.4) contained 119 mM NaCl, 2.5 mM KCl, 1 mM NaH_2PO_4, 26 mM $NaHCO_3$, 1 mM

$MgCl_2$, 25 mM glucose, and 2 mM $CaCl_2$, with an osmolarity of 300-305 mOsm and saturated with 95% O_2 and 5% CO_2. The brain tissue was then subsequently mounted on a custom-made slicing platform with a 10° bevel and sliced into 400 μM coronal sections using a VT1200S vibratome (Leica Biosystems). Following this, the slices were incubated in oxygenated ACSF at 37.0°C ± 0.5°C for 20 minutes, and then incubated at room temperature until being transferred to the recording chamber.

In this experiment, all recordings were from layer 5 pyramidal neurons in the motor cortex. Electrodes were pulled from borosilicate glass using a P-97 puller (Sutter Instruments), with resistances ranging from 4–7 MΩ. The intracellular solution contained 10 mM HEPES, 2.5 mM $MgCl_2$, 20 mM CsCl, 115 mM $CsMeSO_3$, 4 mM Na_2-ATP, 0.4 mM Na-GTP, 10 mM Na-Phosphocreatine, 0.6 mM EGTA and 0.1 mM Spermine (pH 7.25), with an osmolarity of 300 mOsm/kg. A motorized micromanipulator (Junior Multpatch, Lugis & Neumann) was used to guide the electrodes to the target cells for data acquisition. Electrophysiological data acquisition and stimulation commands were managed through synchronized LIH 8+8 data acquisition interface boards (HEKA Instruments), with operation controlled by Igor Pro 6[37].

To study the voltage dependence of slow inactivation, a prepulse was applied for 5 s, stepping from a holding potential of -100 mV to the indicated potentials ranging from -120 mV to 20 mV. Following this, the cells were repolarized to -100 mV for 20 ms to allow recovery from fast inactivation. A second test pulse to 10 mV was then applied for 10 ms, and evoked currents were recorded. To study the onset of slow inactivation, the above protocol was modified so that the prepulse had a fixed voltage (10 mV) but with different durations (ranging from 10 ms to $10^{3.8}$ ms, following an exponential increase pattern). To study the recovery from slow inactivation, both the voltage and the duration of the prepulse were fixed (10 mV, 5 s), but the time interval between the prepulse and the test pulse varied.

Plasmids construction and AAV packaging.

Mouse open reading frame (ORF) of sSLP (Sik3, A260-K527, NM_027498) was produced from Comate Bioscience. The CaMKIIa promoter were from

pAAV-CaMKIIa-hM4D(Gi)-mcherry (Addgene,50477).

Based on previous methods[22,38] for AAV packaging and purification, with some improvements made, pAAV-PHP.eB, pAAV-helper, and the pAAV vector containing the target gene sequence were co-transfected into AAVpro 293T cells using polyethyleneimine "Max" (PEI MAX) transfection reagent. Twelve hours after the transfection, the original culture medium was replaced with serum-free DMEM. After incubating for 5 days, the supernatant was collected and the cells were harvested with a cell scraper. The mixture was then transferred to a 50 ml centrifuge tube and centrifuged at 13,000 rpm for 10 minutes at room temperature. Subsequently, the supernatant was transferred to a new 50 mL centrifuge tube. Meanwhile, the remaining cell pellet was resuspended in 1 ml of phosphate buffered saline (PBS), subjected to 5 freeze-thaw cycles, and then centrifuged at 13,000 rpm for 20 minutes to obtain the supernatant. The supernatants from both centrifugations were filtered through a 0.45 μm filter into a 50 mL centrifuge tube. Next, 6 ml of sterile 14% bovine serum albumin (BSA) were added to reach a final concentration of 3%. Then, 7 ml of pre-chilled PEG8000 solution (4X) were added, mixed thoroughly, and left at 4°C overnight (not exceeding 24 hours). On the following day, the 50 ml centrifuge tube was centrifuged at 3,500 g for 1 hour at 4°C. After that, the supernatant was discarded, and the pellet was centrifuged again at 3,500 g for 1 minute at 4°C. The pellet was then resuspended in 1.5 ml PBS by gentle pipetting. The concentrated virus solution was frozen at -80°C for future use. The virus titers were determined using linearized genomic plasmids as standards. For the injection of AAV virus into mice, the mice were first deeply anesthetized with isoflurane and then injected with 100 μl of AAV virus solution (1.0×10^{12} vg/ml) through the retro-orbital sinus.

Cannula implantation and injection.

In the experiment involving intracerebroventricular injection via cannulation, all the mice were male and were at least 8 weeks old. The mice were kept under continuous anesthesia with isoflurane, and their heads were fixed in a stereotaxic frame to ensure accurate positioning. A stainless cannula was inserted into the right lateral ventricle according to the stereotaxic coordinates of the mouse brain. Given that electrode

implantation was to be carried out after the insertion of the cannula, the angle of cannula insertion was set at 30° to facilitate the subsequent placement of electrodes.

Establishment of the axon initial segment protein database.

Drawing on the GO database, the uniprot database, and relevant literature reports[39], a total of 197 AIS proteins have been collated and presented in Table S1.

Tissue collection and sample preparation for mass spectrometry.

The preparation of mass spectrometry samples was conducted according to previously described procedures with certain modifications[12]. Wild type mice and *N1467D* mice were subjected to two conditions: normal sleep for 6 h (S6) and sleep deprivation for 6 h (SD6). The mice brains were rapidly extracted, placed into cryovials, and immediately frozen in liquid nitrogen. Subsequently, they were transferred to a -80°C freezer for long-term storage. The brain tissue was lysed using a buffer consisting of 50 mM HEPES (pH 8.5), 150 mM NaCl, 2 mM $MgCl_2$, and 1% SDS. A pre-chilled glass homogenizer was used to grind the brain tissue; initially, 5 ml of the brain tissue lysis buffer and nuclease (Thermo) were added, followed by 2 ml of 10% SDS buffer. After homogenization, the samples were incubated for 30 minutes followed by centrifugation at 13,000 g for 20 minutes at room temperature. The supernatant was transferred to a new 15 ml tube. Total protein concentration was determined using the BCA™ Protein Assay (Pierce). Dithiothreitol was added to the protein lysate for reduction, followed by alkylation with iodoacetamide. The samples were then processed using the chloroform-methanol precipitation method and subsequently resuspended in 8 M urea buffer. Following this, the samples were digested with recombinant Lys-C for 2 hours, diluted with 100 mM NH_4HCO_3 buffer (pH 7.8) to a final concentration of 2 M urea, and further digested with trypsin (Promega) at room temperature for 12 hours. The digestion was terminated with 1% trifluoroacetic acid (TFA). The resulting peptides were desalted using C18 solid-phase extraction and then concentrated to near dryness by vacuum centrifugation.

The desalted peptides were resuspended in 1.2 ml of phosphopeptide binding buffer [2 M lactic acid/50% acetonitrile (ACN)], and centrifuged at 13,000 g for 20 minutes. The supernatant was transferred to a new tube. TiO_2 beads were first washed three

times with the phosphopeptide binding buffer, then added to the supernatant and incubated at room temperature for 1 hour. The mixture was then washed twice with 2 M lactic acid/50% ACN, followed by two washes with 50% ACN/0.1% TFA. Elution was performed twice with 500 µL of elution buffer (50 mM K_2HPO4, pH 10), followed by acidification with 20% TFA, desalting, and concentration to dryness by vacuum centrifugation.

The enriched phosphopeptides were resuspended in 200 mM HEPES (pH 8.5) buffer. The concentration of phosphopeptides was determined using the BCA assay. Approximately 50 µg of each sample was labeled with Tandem Mass Tags (TMT) at room temperature for 1 hour. Labeling was quenched with 5% hydroxylamine, and the TMT-labeled samples were pooled into a single tube, acidified with 20% TFA, desalted, and concentrated to near dryness by vacuum centrifugation. The samples were then subjected to HPLC fractionation using a 400 µl buffer A (1% ACN, 10 mM ammonium formate, pH 9.5) and an Agilent 300 Extend C18 column (5 µm particles, 4.6 mm inner diameter, 150 mm length). After HPLC fractionation, the samples were acidified with 20% TFA and concentrated to dryness by vacuum centrifugation. The resulting samples were desalted using Stage Tips, concentrated to dryness, and resuspended for LC/MS analysis.

Mass spectrometry data acquisition and processing.

For liquid chromatography tandem mass spectrometry (LC-MS/MS) analysis, TMT-labeled peptides were separated using a 120-minute gradient elution at a flow rate of 0.300 mL/min through an Ultimate 3000 system, which was connected directly to a Thermo Orbitrap exploris 480 mass spectrometer. The analytical column was a fused silica capillary (75 µm ID, 150 mm long; Upchurch, Oak Harbor, WA) packed with C-18 resin (300 Å, 5 µm; Varian, Lexington, MA). Mobile phase A consisted of 0.1% formic acid, and mobile phase B consisted of 100% acetonitrile and 0.1% formic acid. The Orbitrap exploris 480 mass spectrometer was operated in data-dependent acquisition mode using Xcalibur 4.5 software. The Orbitrap performed a single full-scan mass spectrometry analysis (300-1800 m/z, 60,000 resolution), followed by a 2 s of data-dependent MS/MS scans in an ion-guided

multipole with a standard collision energy of 36%.

Mass spectra obtained from each LC-MS/MS analysis were compared with the mouse database using the Sequest HT algorithm in Proteome Discoverer software (PD, version 2.5). The search criteria were as follows: complete trypsin specificity was required; one missed cut was allowed; oxidation (M) was set to variable modification; carbamidomethylation (C) and TMTsixplex (K- and N-terminal) were set to fixed modification; and the precursor ion mass tolerance was set to 20 ppm for all MS data and 0.02 Da for all MS/MS spectra. Peptide False Discovery Ratio (FDR) was calculated using Percolator provided with PD 2.5. Peptide spectra were considered correctly matched when the q value was less than 1%. Relative protein quantification was performed by PD software based on the intensity of TMT reporter ions. Quantification was performed only for proteins with two or more unique peptide matches. Peptides assigned to only a single proteome were considered unique. Protein ratios were calculated based on the median number of all peptides belonging to the protein. The precision of quantification is expressed by the variability of the protein ratios.

Mass spectrometry data analysis.

Protein isoforms were considered distinct proteins in proteomic analysis. Phosphopeptides were utilized in phosphoproteomic analysis, which includes unique forms and composite forms (containing two or more phosphorylation sites). Standardized abundance data obtained from experiments are combined (summed) to generate unique protein or phosphopeptide IDs along with the aggregated abundance values, which are then scaled to ensure that the average abundance for each sample is one. Standardized data from different experiments were integrated based on a unique sample ID for comparative purposes (e.g., SD6-WT/S6-WT). Subsequently, the "$\log_2$(fold change)" values were generated using the means of each experimental group; statistical significance ($P < 0.01$ or $P < 0.02$) was analyzed through multiple unpaired t-tests (*P*-values). Detailed descriptions and datasets of all phosphoproteomic experiments are listed in Table S5, while datasets from all proteomic experiments are listed in Table S5.

The calculation method for the change in phosphorylation state (ΔPs) value is as previously described[12], which is equal to the sum of the "$\log_2$(fold change)" values of all phosphorylated peptides that show statistically significant changes ($P < 0.02$). These phosphorylated peptides come from all protein isoforms encoded by the same gene. If none of the P values for the phosphorylated peptides are less than 0.02, then the ΔPs value is zero. A complete description of the ΔPs analysis and the dataset are listed in Table S6.

Kinase substrate site prediction and kinase enrichment analysis.

The kinase prediction of phosphorylation sites was performed using the Group-based Prediction System (GPS)[24]. The kinase enrichment analysis was conducted following the methodology described in the cited literature[28]. The sites to be predicted were converted into sequence format, and a 15-amino acid sequence encompassing each site was extracted. Subsequently, this sequence was entered into the website https://kinase-library.phosphosite.org, and kinase predictions were made based on whether the site belonged to PKA, PKC, or sleep kinases, with a binding score exceeding 95. The kinase analysis was generated using these criteria. The predicted results are organized in Table S7.

Novel object recognition (NOR).

The experiment mainly consists of three stages[40]. Data recording and analysis were conducted using Smart 3.0 video tracking software (Panlab Harvard Apparatus). The first stage serves as an adaptation process that is repeated over the course of three days. A square empty wooden board is placed on the floor, and then the mice are placed inside to freely explore for 10 minutes. After each mouse finishes exploring, the wooden board is wiped with 75% alcohol to wipe off the scent left by the previous mouse. The second stage acts as the training phase. Two objects with the same shape and color are positioned diagonally within the empty arena. The mice are placed in the center of the arena, at an equal distance from the two objects. They are allowed to explore for ten minutes, during which the time spent on moving and contacting the two objects is recorded. Between each mouse experiment, the wooden board and the objects are thoroughly cleaned using 75% ethanol. The third stage marks the testing

period. After three hours of training, one of the objects with a different shape and color is substituted for the previous one in the same arena. The mice are again placed in the center of the arena, equidistant from the two objects. They are permitted to freely explore for ten minutes, and the distance they travel as well as the time they spend in contact with the two objects are recorded. The discrimination index is calculated by comparing the exploration time of the mice towards the new object and the familiar object, with the intention of evaluating their short-term memory and recognition abilities.

Morris water maze (MWM).

The water maze apparatus was positioned in a controlled environment with moderate lighting, as described previously[41]. The water maze consisted of a circular pool filled with water to a depth of approximately 30-40 cm. A non-toxic white pigment, titanium dioxide, was added to the pool to improve the visibility for the mice. The pool was divided into four quadrants. Meanwhile, the inner area of the water maze was equipped with four distinct markers in different shapes. A circular hidden platform, located in the center of the third quadrant, was placed about 1-2 cm beneath the water surface and had a diameter of 10-12 cm. The position of this platform remained unchanged throughout the experiment. Before the experiment commenced, the water temperature was maintained at around 24 °C to minimize the stress responses of the mice. Data recording and analysis were conducted using Smart 3.0 video tracking software (Panlab Harvard Apparatus).

The water maze experiment comprised adaptation, learning, and testing phases. Prior to the formal commencement of the experiment, the mice were permitted to swim freely in the pool to adapt themselves to the environment. The learning phase lasted for five days, starting at 9 am each day. During this period, each mouse went through four training trials. In these trials, the mice were placed into the water from the same position with their heads facing the wall of each of the four quadrants. Each trial had a time limit of 60 s for swimming. If a mouse failed to find the platform within this time limit, the experimenter would guide it onto the platform and ask the mouse to stay

there for 15 s to assist in the formation of memory regarding the platform's location. The testing phase was carried out on the sixth day. During this day, the platform was removed from the pool. Subsequently, the mice were placed into the water from the first quadrant with their heads facing the wall. The time it took for each mouse to find the platform was recorded, along with the number of times the mouse crossed the platform within 60 s and the duration that the mouse spent in the third quadrant. After each experimental session, both the pool and the platform were cleaned to eliminate any residual odor.

Statistical methods.

All experiments were carried out with biological replicates, and each experiment was independently conducted at least twice to ensure the reliability. The schematics were created using BioRender. Mice were randomly assigned numbers and blindly grouped for EEG/EMG, novel object recognition, and water maze experiments, as well as subsequent data processing. The intensity of protein bands was quantified using Image J software. Statistical analysis was performed using GraphPad Prism and EXCEL software. Two-way analysis of variance (ANOVA) was employed, followed by Sidak's test for comparing multiple means, Fisher's LSD test for pairwise mean comparisons when ANOVA shows significant differences between groups. The complete sample size, statistical analysis methods, and results for each comparison are reported in the figure legends and Table S8.

Reference

1 Funato, H. *et al.* Forward-genetics analysis of sleep in randomly mutagenized mice. *Nature* **539**, 378-383 (2016)

2 Park, M. *et al.* Loss of the conserved PKA sites of SIK1 and SIK2 increases sleep need. *Sci Rep* **10**, 8676 (2020)

3 Mikhail, C., Vaucher, A., Jimenez, S. & Tafti, M. ERK signaling pathway regulates sleep duration through activity-induced gene expression during wakefulness. *Sci Signal* **10** (2017)

4 Kon, K. *et al.* Cortical parvalbumin neurons are responsible for homeostatic sleep rebound through CaMKII activation. *Nat Commun* **15**, 6054 (2024)

5 Tatsuki, F. *et al.* Involvement of Ca(2+)-Dependent Hyperpolarization in Sleep Duration in Mammals. *Neuron* **90**, 70-85 (2016)

6 Hellman, K., Hernandez, P., Park, A. & Abel, T. Genetic evidence for a role for protein kinase A in the maintenance of sleep and thalamocortical oscillations. *Sleep* **33**, 19-28 (2010)

7 Wang, Y. *et al.* Postsynaptic competition between calcineurin and PKA regulates mammalian sleep-wake cycles. *Nature* **636**, 412-421 (2024)

8 Brüning, F. *et al.* Sleep-wake cycles drive daily dynamics of synaptic phosphorylation. *Science* **366** (2019)

9 Pinto, M. J. *et al.* Microglial TNFα orchestrates protein phosphorylation in the cortex during the sleep period and controls homeostatic sleep. *Embo j* **42**, e111485 (2023)

10 Tsai, Y. C. *et al.* Modulation of sleep/wake patterns by gephyrin phosphorylation status. *Eur J Neurosci* **60**, 5431-5449 (2024)

11 Diering, G. H. *et al.* Homer1a drives homeostatic scaling-down of excitatory synapses during sleep. *Science* **355**, 511-515 (2017)

12 Wang, Z. *et al.* Quantitative phosphoproteomic analysis of the molecular substrates of sleep need. *Nature* **558**, 435-439 (2018)

13 Cirelli, C. & Tononi, G. Linking the need to sleep with synaptic function. *Science* **366**, 189-190 (2019)

14 Hu, W. *et al.* Distinct contributions of Na(v)1.6 and Na(v)1.2 in action potential initiation and backpropagation. *Nat Neurosci* **12**, 996-1002 (2009)

15 Studtmann, C., Ladislav, M., Topolski, M. A., Safari, M. & Swanger, S. A. Na(V)1.1 haploinsufficiency impairs glutamatergic and GABAergic neuron function in the thalamus. *Neurobiol Dis* **167**, 105672 (2022)

16 Krone, L. B. *et al.* A role for the cortex in sleep-wake regulation. *Nat Neurosci* **24**, 1210-1215 (2021)

17 Vyazovskiy, V. V. & Harris, K. D. Sleep and the single neuron: the role of global slow oscillations in individual cell rest. *Nat Rev Neurosci* **14**, 443-451 (2013)

18 Cantrell, A. R. *et al.* Molecular mechanism of convergent regulation of brain Na(+) channels by protein kinase C and protein kinase A anchored to AKAP-15. *Mol Cell Neurosci* **21**, 63-80 (2002)

19 Chen, Y., Yu, F. H., Surmeier, D. J., Scheuer, T. & Catterall, W. A. Neuromodulation of Na+ channel slow inactivation via cAMP-dependent protein kinase and protein kinase C. *Neuron* **49**, 409-420 (2006)

20 Planells-Cases, R. *et al.* Neuronal death and perinatal lethality in voltage-gated sodium channel alpha(II)-deficient mice. *Biophys J* **78**, 2878-2891 (2000)

21 Ushimaru, M. & Kawaguchi, Y. Temporal Structure of Neuronal Activity among Cortical Neuron Subtypes during Slow Oscillations in Anesthetized Rats. *J Neurosci* **35**, 11988-12001 (2015)

22 Chan, K. Y. *et al.* Engineered AAVs for efficient noninvasive gene delivery to the central and peripheral nervous systems. *Nat Neurosci* **20**, 1172-1179 (2017)

23 Xu, J. *et al.* Regulation of sleep quantity and intensity by long and short isoforms of SLEEPY kinase. *Sleep* **45** (2022)

24 Chen, M. *et al.* GPS 6.0: an updated server for prediction of kinase-specific phosphorylation sites in proteins. *Nucleic Acids Res* **51**, W243-w250 (2023)

25 Rossie, S., Gordon, D. & Catterall, W. A. Identification of an intracellular domain of the sodium channel having multiple cAMP-dependent phosphorylation sites. *J Biol Chem* **262**, 17530-17535 (1987)

26 Tibbs, V. C., Gray, P. C., Catterall, W. A. & Murphy, B. J. AKAP15 anchors cAMP-dependent protein kinase to brain sodium channels. *J Biol Chem* **273**, 25783-25788 (1998)

27 Polishchuk, A. *et al.* Synaptic retrograde regulation of the PKA-induced SNAP-25 and Synapsin-1 phosphorylation. *Cell Mol Biol Lett* **28**, 17 (2023)

28 Johnson, J. L. *et al.* An atlas of substrate specificities for the human serine/threonine kinome. *Nature* **613**, 759-766 (2023)

29 Filipis, L. *et al.* Nav1.2 and BK channel interaction shapes the action potential in the axon initial segment. *J Physiol* **601**, 1957-1979 (2023)

30 Kaczmarek, L. K. Loss of Na(V)1.2-Dependent Backpropagating Action Potentials in Dendrites Contributes to Autism and Intellectual Disability. *Neuron* **103**, 551-553 (2019)

31 Menezes, L. F. S., Sabiá Júnior, E. F., Tibery, D. V., Carneiro, L. D. A. & Schwartz, E. F. Epilepsy-Related Voltage-Gated Sodium Channelopathies: A Review. *Front Pharmacol* **11**, 1276 (2020)

32 Middleton, S. J. *et al.* Altered hippocampal replay is associated with memory impairment in mice heterozygous for the Scn2a gene. *Nat Neurosci* **21**, 996-1003 (2018)

33 Jain, S. V., Panjeton, G. D. & Martins, Y. C. Relationship Between Sleep Disturbances and Chronic Pain: A Narrative Review. *Clin Pract* **14**, 2650-2660 (2024)

34 Pandi-Perumal, S. R. *et al.* Clarifying the role of sleep in depression: A narrative review. *Psychiatry Res* **291**, 113239 (2020)

35 Lou, T. *et al.* Hyper-Activation of mPFC Underlies Specific Traumatic Stress-Induced Sleep-Wake EEG Disturbances. *Front Neurosci* **14**, 883 (2020)

36 Shi, Y. & Wang, G. Protocol to study microcircuits in the medial entorhinal cortex in mice using multiple patch-clamp recordings and morphological reconstruction. *STAR Protoc* **5**, 102917 (2024)

37 Wang, G. *et al.* An optogenetics- and imaging-assisted simultaneous multiple patch-clamp recording system for decoding complex neural circuits. *Nat Protoc* **10**, 397-412 (2015)

38 Wang, G. *et al.* Somatic Genetics Analysis of Sleep in Adult Mice. *J Neurosci* **42**, 5617-5640 (2022)

39 Zhang, W. *et al.* Immunoproximity biotinylation reveals the axon initial segment proteome. *Nat Commun* **14**, 8201 (2023)

40 Lueptow, L. M. Novel Object Recognition Test for the Investigation of Learning and Memory in Mice. *J Vis Exp* (2017)

41 Shao, Q. *et al.* A non-canonical visual cortical-entorhinal pathway contributes to spatial navigation. *Nat Commun* **15**, 4122 (2024)